American Mineralogist, Volume 102, pages 1922–1933, 2017

Phase relations and formation of K-bearing Al-10 Å phase in the MORB+H_2O system: Implications for H_2O- and K-cycles in subduction zones

Renbiao Tao[1], Lifei Zhang[1,*], Xi Liu[1], Thomas Bader[1], and Yingwei Fei[1,2]

[1]The MOE Key Laboratory of Orogenic Belt and Crustal Evolution, School of Earth and Space Sciences, Peking University, Beijing 100871, China
[2]Geophysical Laboratory, Carnegie Institution of Washington, Washington, D.C. 20015, U.S.A.

Abstract

The potassium (K) and water (H_2O) cycles in subduction zones are predominately controlled by the stability of K- and H_2O-bearing minerals, such as K-mica, lawsonite, and dense hydrous magnesium silicates (DHMS). K-micas (muscovite or phlogopite) are the principal H_2O and K hosts in subduction zones and Earth's upper mantle and play a significant role in the deep H_2O and K cycles. The Mg-10 Å phase, normally appearing in hydrated peridotite in high-pressure experiments, has been considered as an important water-carrier in subducted hydrated peridotite. In this study, we found a K-bearing Al-10 Å phase in the MORB+H_2O system (hydrated basalt) at high pressures according to X-ray diffraction and stoichiometry. We experimentally constrained its stability field at high pressure. By considering newly and previously documented compositions of the 10 Å phase and micas, we confirmed a continuous solid solution or mixed layering between the 10 Å phase and K-mica at the interlayer site, suggesting that the K cycle and the H_2O cycle in subduction zones are coupled. From the discussion of the effect of f_{H_2O} on stability of the Al-10 Å phase, we conclude that a cold subduction zone can host and carry more bulk H_2O and K into Earth's deep mantle than a hot one. This work expands the stability regions of the 10 Å phase from the ultramafic system (Mg-10 Å phase) to the mafic system (Al-10 Å phase), and emphasizes the significance of the 10 Å phase for the deep H_2O and K cycle in subduction zone.

Keywords: H_2O- and K-cycle, Al-10 Å phase, K-mica, high pressure, subduction zone

Introduction

Subduction zone fluids play an important role in metamorphism of subducted slabs, the slab-mantle interaction, and the generation of arc magmas (Peacock and Wang1999; Schmidt and Poli 1998; Padrón-Navarta et al. 2010). Water can be carried into deep Earth by various hydrous minerals (e.g., amphibole, lawsonite, mica, and DHMS) in a subduction zone and released from the subducted slab via dehydration to trigger melting of the mantle wedge and the production of arc magmas (Wyllie 1988; Tatsumi and Eggins 1995; Poli and Schmidt 2002; Kawamoto 2006; Hacker 2008). The oceanic basaltic crust, with a bulk composition equivalent to MORB or OIB, is commonly altered to greenschist facies by hydrothermal activity and subsequent interaction with sea water during residence on the oceanic floor (Miyashiro 1973; Alt 1995). The principal hydrous phases in the altered oceanic crust are amphibole, chlorite, zoisite, and clay minerals (Tatsumi and Eggins 1995; Alt 1995; Staudigel 2014). During subduction into Earth's mantle, the dehydration of hydrous minerals in the subducted slab strongly depends on the stability of water-bearing minerals, the subduction depth, and the thermal structure of the subduction zone (Van Keken et al. 2011; Schmidt and Poli 2014). Altered oceanic crust may evolve from greenschist through amphibolite to dry eclogite along a hot subduction path and the accompanying phase relations and dehydration behavior have been widely studied and reviewed (Maruyama and Okamoto 2007; Schmidt and Poli 2014 and reference therein). The isobaric amphibole breakdown at ~2.5 GPa, traditionally defining the amphibolite-eclogite-transition, has been held responsible for mass transfer triggering arc magmatism above hot subduction zones (Wyllie 1988; Tatsumi and Eggins 1995). However, most subduction zones, especially in the Phanerozoic ones, usually transforms from lawsonite blueschist to lawsonite eclogite along cold subduction path (Brown 2006; Syracuse et al. 2010; Tsujimori and Ernst 2014). The phase relations from lawsonite blueschist to lawsonite eclogite in cold subduction zone are still not very clear.

Lawsonite, $CaAl_2Si_2O_7(OH)_2 \cdot H_2O$, a hydrous index mineral for low-temperature metamorphism, normally occurs in hydrated basaltic rocks at lawsonite blueschist and lawsonite eclogite facies (Maruyama et al. 1996; Poli and Schmidt 2002). Its stability, 3 to 10 GPa below ~800 °C, has been experimentally determined in the MORB+H_2O system (Schmidt 1995; Okamoto and Maruyama 1999). Until now, only about 10 lawsonite eclogite occurrences have been documented worldwide, in contrast to the vast number of Phanerozoic cold subduction orogenic belts (Tsujimori et al. 2006). Lawsonite eclogites are rare because of the difficulty of lawsonite preservation during exhumation (Clarke et al. 2006; Whitney and Davis 2006; Wei and Clarke 2011). That is why little attention has been paid to the phase relations in lawsonite eclogites.

The 10 Å phase, $Mg_3Si_4O_{10}(OH)_2 \cdot nH_2O$, was synthesized in a simple MgO-SiO_2-H_2O (MSH) system by Bauer and Sclcar (1981) and in a hydrated peridotite system by Fumagalli and

* E-mail: Lfzhang@pku.edu.cn

0003-004X/17/0009–1922$05.00/DOI: http://dx.doi.org/10.2138/am-2017-6025

Poli (2005). It can contain as much as 13.6 wt% H_2O (Welch et al. 2006; Fumagalli and Stixrude 2007). Under high water-saturation conditions, talc can transform into the 10 Å phase at pressures between 3 and 5 GPa through the reaction talc + H_2O = 10 Å phase (Pawley and Wood 1995; Chinnery et al. 1999). The 10 Å phase is stable at pressures up to 9.5 GPa, above which it transforms into another hydrous phase, the 3.65 Å phase, in the MgO-SiO_2-H_2O system (Pawley et al. 2011). Due to its significance for the deep H_2O cycle, the physical and chemical properties of the 10 Å phase at high pressure have been widely investigated theoretically (Wang et al. 2004; Fumagalli and Stixrude 2007) and experimentally (Fumagalli et al. 2001; Comodi et al. 2005, 2006; Welch et al. 2006; Chollet et al. 2009; Pawley et al. 2010, 2011). A phlogopite-type layer structure has been proposed for the 10 Å phase on the basis of neutron powder diffraction on deuterated crystals (Pawley et al. 2004) and structure refinement via X-ray diffraction (Fumagalli et al. 2001; Comodi et al. 2005). Fumagalli and Poli (2005) reported a the 10 Å phase containing about 10 wt% Al_2O_3 in experiments on hydrous K-free peridotites, which was confirmed by Dvir et al. (2010). Complex interlayering between the 10 Å phase and chlorite has been suggested to account for this peculiar mineral chemistry. Fumagalli et al. (2009) experimentally studied alkalis in phlogopite in metasomatized, K-doped peridotites at high pressure and a possible mixed layering or solid solution between the 10 Å phase and phlogopite was suggested to account for K contents as low as 0.3 pfu in phlogopite formed at low-temperature and high-pressure conditions. Given that talc is a widespread low-temperature and high-pressure mineral in hydrated oceanic crusts, especially in hydrous Mg-gabbro crust (Liou and Zhang 1995; Massonne 2004; Bucher and Grapes 2009; Wei and Clarke 2011), it is likely that talc would transform into the 10 Å phase in a hydrous basalt at water-saturation and high-pressure conditions. Our experimental study will focus on the formation of the 10 Å phase in hydrated basalt in a cold subduction environment.

K-micas (muscovite and phlogopite) are the principal H_2O and K hosts in subduction zones and Earth's upper mantle, they are significant for studying the deep H_2O- and K-cycle. A systematic increase of the K content of volcanic arc magmas with the depth of the Wadati-Benioff-Zone below arc volcanoes is common. This observation is attributed to the stability of K-bearing minerals (such as K-mica) in the subducting slab (Dickinson and Hatherton 1967; Ringwood 1974; Tamura et al. 2007). The understanding of the properties of K-mica can reveal the mechanisms transporting H_2O and K into Earth's mantle and generating K-bearing volcanic arc magmas in the subduction zones. For example, phengite is able to transport K and H_2O down to 300 km depth and will transfer to K-hollandite above 10 GPa (Schmidt 1996). Dehydration or melting of phengite in the subduction zone could liberate K-rich fluids or melts—the metasomatic agents for the generation of calc-alkaline arc magmas in the mantle wedge (Domanik and Holloway 1996; Schmidt 1996; Tamura et al. 2007). When these K-rich fluids or melts interact with ultramafics at the slab-mantle interface, some H_2O and K will be re-stored in phlogopite in the metasomatized mantle (Wunder and Melzer 2003; Fumagalli et al. 2009; Mallik et al. 2015). Proceeding within the mantle wedge and at the slabs-mantle interface, this process is reflected by phlogopite-spinel peridotites, phlogopite-garnet peridotites, and orogenic phlogopite peridotites in UHP terrains [e.g., Sulu garnet peridotite, China: Zhang et al. (2007); Ulten peridotite: Rampone and Morten (2001); Bardane peridotite: van Roermund et al. (2002)]. Recently, Mallik et al. (2015) also experimentally confirmed that slab-derived melt reacts with peridotite to form a phlogopite-bearing pyroxenitic residue. Other experiments have shown that phlogopite can be stable up to 6–7 GPa at 1100 °C in lherzolite and its breakdown is controlled by appearance of K-richterite (Konzett and Ulmer 1999), which will be replaced by Phase X ($K_{2-x}Mg_2Si_2O_7H_x$ with x = 0–1), at approximately 12–13 GPa, 1200 °C (Konzett and Fei 2000). At sub-solidus conditions, Fumagalli et al. (2009) inferred that a solid solution or mixed layering of phlogopite and the 10 Å phase is an important H_2O and K host at relatively low temperatures and high pressures in metasomatized peridotite. However, there has been no systematic study on the stability of K- and H_2O-bearing phases in hydrous basalts at sub-solidus conditions.

To understand the geochemical behavior of K and H_2O in hydrous basalt in a cold subduction zone, we designed and carried out a series of high-pressure experiments on a natural lawsonite blueschist (Supplemental[1] Fig. 1; Supplemental[1] Table 1) along cold subduction path. To compare the results with the stability of phlogopite in hydrous peridotite system, and to determine if the 10 Å phase could be stable in hydrous basalt system, our experimental conditions overlap with those used in previous studies in hydrous peridotite system (Fumagalli and Poli 2005; Fumagalli et al. 2009).

Experimental procedures

Starting material

In this study, a natural lawsonite blueschist (2S46) from the Early Paleozoic low-temperature and high-pressure metamorphic belt in the North Qilian Mountains, NW China, was selected as starting material (Song et al. 2005). Its bulk composition was obtained by X-ray fluorescence (XRF) at the MOE Key Laboratory of Orogenic Belts and Crustal Evolution, Peking University. Compared with the global average MORB compositions (McDonough 2014) and starting materials previously used for experiments on lawsonite (Okamoto and Maruyama 1999) and phengite (Schmidt 1996) in the MORB+H_2O system, the starting material in this study contains more Na_2O (6.81 wt%, outside the range of altered MORB), less CaO (4.2 wt%), and similar K_2O (Supplemental[1] Table 1). The natural starting material contains ~5.6 wt% bulk water (L.O.I.; Supplemental[1] Table 1), consistent with the experimentally estimated water content of blueschists (5–6 wt%) in the MORB+H_2O system (Schmidt and Poli 1998; Okamoto and Maruyama 1999). No additional water was added in the experiments. The modal proportions (vol%) of each mineral in the lawsonite blueschist were visually estimated under the optical microscope by Zhang et al. (2009) and this study (Supplemental[1] Table 2): it predominantly consists of lawsonite, glaucophane, chlorite, albite, and quartz, with minor amount of garnet (<2 vol%; Supplemental[1] Fig. 1). The starting material contains more than 90 vol% of water-bearing minerals (glaucophane, lawsonite, and chlorite) and about 48 vol% of Na-rich minerals (Na-amphibole and albite). The CaO of the starting material is almost entirely hosted by lawsonite. Revealed by thermodynamic calculations, the lawsonite blueschist experienced a peak metamorphism at 335–355 °C and 0.8–0.95 GPa, *P-T* conditions at the transition from the lawsonite blueschist to the epidote blueschist facies (Zhang et al. 2009).

Experimental conditions and apparatus

The starting material was finely ground (<200 mesh) in an agate mortar under ethanol. To simulate the natural situation in the subduction zone and enable the escape

[1]Deposit item AM-17-96025, Supplemental Figures and Tables. Deposit items are free to all readers and found on the MSA web site, via the specific issue's Table of Contents (go to http://www.minsocam.org/MSA/AmMin/TOC/2017/Sep2017_data/Sep2017_data.html).

of any H_2O liberated by dehydration, for each experiment, the fine starting material was sandwiched between diamond powder (grain size: 30–40 μm, Alfa Aesar, A Johnson Matthey Company; ~0.5 mm thick) in an unsealed platinum tube (outer diameter = 3 mm, length = ~2.5 mm) (Fig. 1). Before the sample loading, the platinum tubes were boiled in diluted HCl for 30 min, ultrasonically cleaned in ethanol for 10 min, and then stored in an oven at 110 °C. To evaluate the influence of fluid migration on the stability and properties of hydrous minerals at high pressure, we performed two additional experiments in sealed platinum capsules at 4 and 5.5 GPa. For the sealed-capsule experiments, the sample-loaded capsule was arc-welded. In both kinds of capsules, the starting materials are in direct contact with the Pt capsule, which was not pre-saturated with Fe. Iron loss to the capsule may occur depending on the conditions of the experiments (Johannes and Bode 1978).

All high-pressure experiments were performed at pressures from 3.5 to 8 GPa and temperatures of 600 to 900 °C at the High Pressure High Temperature Lab of Peking University, using a CS-IV 6 × 14 MN cubic press. The press consists of six tungsten carbide (WC) anvils, with 23.5 × 23.5 mm^2 sized truncated tips, which are simultaneously pushed by six hydraulic rams. The press can produce stable pressures up to about 10 GPa with three well-calibrated experimental assemblies (Liu et al. 2012a). For experimental runs below and above 6 GPa, the assemblies BJC-1 (Fig. 1) and BJC4-6 were used, respectively. The cell pressures were determined by using the phase transition points of Bi (I–II at 5.5 GPa, II–III at 2.69 GPa, and III–V at 7.7 GPa), Ba (I–II transition at 5.5 GPa), and ZnFe (band gap change at 6.6 GPa and I–II transition at 8.9 GPa). Details of the cell assemblies and calibrations have been described in a previous publication (Liu et al. 2012b). The pressure uncertainties, which largely depend on the accuracy of the calibration reaction, were estimated to be <3%. The experimental temperature was measured and controlled with a $Pt_{94}Rh_6$-$Pt_{70}Rh_{30}$ thermocouple (type B), ignoring the pressure effect on its e.m.f. The temperature gradients are less than 15 °C as checked in a test run at 1200 °C by three thermocouples located on the top, middle, and bottom of the BN pressure medium in the graphite heater. Both pressures and temperatures were automatically controlled during the entire experiments. Samples were first pressurized to the target pressure, then heated at a rate of 100 °C/min, and finally held at the target temperature for sufficient time to reach equilibrium (Supplemental[1] Table 2). Each experiment was quenched by shutting off the power supply to the furnace, followed by automatic decompression to atmospheric pressure.

To identify phases and mineral assemblages of the run products, a piece of the recovered sample was mounted in epoxy resin, and polished for analyses with scanning electronic microscopy (SEM) and electron probe microanalysis (EPMA). The remaining sample materials were ground in an agate mortar under ethanol before obtaining powder X-ray diffraction patterns (XRD).

The powder XRD patterns were collected with an X'Pert Pro MPD X-ray diffractometer operated at 40 kV and 40 mA with Cu$K\alpha$ radiation. To obtain high-resolution powder XRD pattern for analysis of the crystal structure of the new phase (the Al-10 Å phase), we used a collecting time of 60 min. The XRD patterns were analyzed with the Jade 6.0 software and compared with standard X-ray PDF data (International Centre for Diffraction Data) to identify phases. For the new phase-bearing experimental products (BE-3 and BE-4), we refined the lattice parameter of the new phase using the GSAS software package (Larson and Von Dreele 2004). The BSE images and EDS spectra were collected on the polished sections with a high-resolution field emission Quanta 650 FEG SEM operated at 15 kV, equipped with an Oxford INCA X-MAX50 250+ EDS. The quantitative chemical compositions of the run products were analyzed with a JEOL JXA-8800R electron microprobe operated at 15 kV accelerating voltage and 20 nA beam current, with a beam diameter of 2 μm and counting time of 20–30 s. Synthetic silica (Si) and spessartine (Mn), and natural pyrope (Mg), andradite (Fe, Ca), albite (Na, Al), rutile (Ti), and sanidine (K) were used as standards. Data were reduced with a ZAF correction program. All the analyses were performed at the MOE Key Laboratory of Orogenic Belt and Crustal Evolution, Peking University.

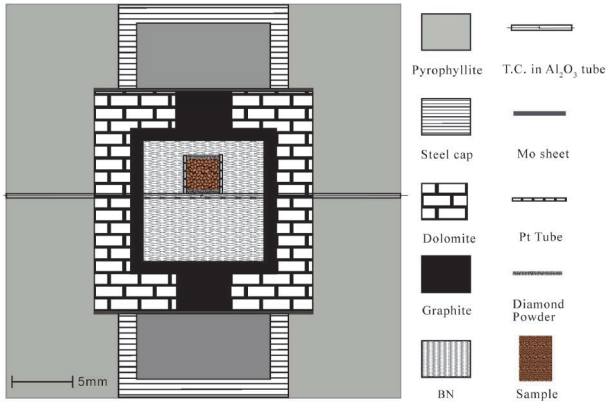

Figure 1. Experimental assembly (BJC-1) with the cubic press CS-IV 6 × 14 MN installed at the High-pressure Laboratory, Peking University. The starting materials are sandwiched between diamond powder in a Pt tube. (Color online.)

Experimental equilibrium

The use of natural minerals as the starting material poses challenge for the achievement of equilibrium, especially at low temperatures. At a temperature of 650 °C, we performed experiments up to 200 h (Supplemental[1] Table 2) to ensure equilibrium by sufficiently long experimental duration. Reversals in such a complex system are particularly difficult if not impossible. For the highest temperature runs (900 °C), 50 h heating was sufficient to equilibrate the experiment, in comparison to 24 h heating used in a previous study in a similar chemical system (Kogiso et al. 1997). For experimental temperatures below 800 °C, we increased the heating duration to more than 100 h according to the Arrhenius equation of temperature dependence of reaction rates. The BSE images indicated that most high-temperature experiments (≥800 °C) have reached equilibrium, while some lower temperature (≤700 °C) runs have indications of local disequilibrium (Fig. 2).

Results

Phase assemblages

Altogether, we conducted 12 high-pressure and high-temperature experiments to determine the phase relations on a lawsonite blueschist from 3.5 to 8 GPa at temperatures of 600 to 900 °C. Experimental conditions and run products are summarized in Supplemental[1] Table 2. The phase proportions of run products were determined by a combination of visual estimates from BSE images (e.g., Fig. 2) and mass-balance calculations on the basis of bulk composition and mineral compositions.

The lowest experimental pressure applied in this study is 3.5 GPa at 650 °C (BE-9). Compared with the starting material, the major changes are disappearance of chlorite and albite, and appearance of more garnet and heterogeneous Na-clinopyroxene (Fig. 2a). A small amount of epidote was observed in the high-temperature part of the capsule. The main mineral assemblage changed to glaucophane (30%), lawsonite (28%), garnet (15%), Na-clinopyroxene (25%), and epidote (2%). Because the total amount of garnet and Na-clinopyroxene in this experimental product is still lower than 50%, and lawsonite and glaucophane are still stable, the mineral assemblage in this run product is still attributed to the lawsonite blueschist facies.

At 4 GPa, we carried out two experiments (BE-1-1 and BE-1-2) at 650 °C with different capsules: BE-1-2 in a sealed platinum capsule and BE-1-1 in a diamond powder-sandwiched platinum tube. Both yielded the same mineral assemblages consisting of garnet, Na-clinopyroxene, lawsonite, and a new water- and K-bearing phase: the Al-10 Å phase (details are discussed later in the mineral chemistry part), but with different mineral proportions (Supplemental[1] Table 2). Both experimental products contain more than 75% (garnet+Na-clinopyroxene), ~10% lawsonite, and 5–15% of the Al-10 Å phase, yet no glaucophane was observed. The observed assemblage represents the lawsonite eclogite facies. The compositions of Na-clinopyroxenes are also heterogeneous in both experiments due to low experimental temperature. The closed system experiment produced more

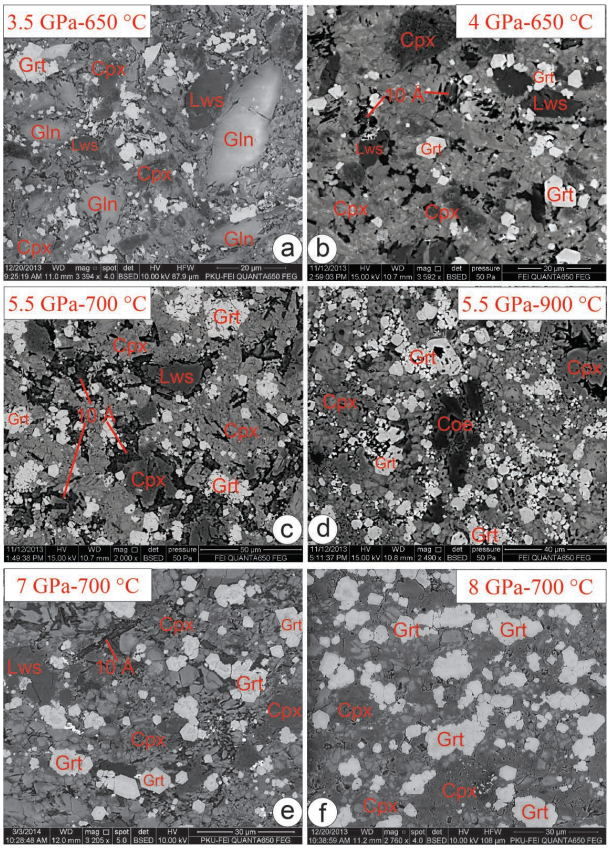

Figure 2. Selected backscattered electron (BSE) images of representative experimental products, with experimental conditions indicated on the figures. (**a**) Run BE-9: Coarse-grained glaucophane in a fine-grained matrix of garnet, Na-clinopyroxene, and small amount of lawsonite. (**b**) Run BE-1: Fine-grained Al-10 Å phase in a lawsonite-bearing garnet - Na-clinopyroxene assemblage. (**c**) Run BE-3: Medium-grained Al-10 Å phase in a lawsonite-bearing garnet–Na-clinopyroxene assemblage. (**d**) Run BE-5: Coesite in a garnet–Na-clinopyroxene assemblage. (**e**) Run BE-13: Fine-grained Al-10 Å phase and lawsonite in a garnet–Na-clinopyroxene assemblage. (**f**) Run BE-8: Homogeneous coesite-bearing garnet–omphacite assemblage. The mineral abbreviation follows Whitney and Evans (2009) in all figures. (Color online.)

and bigger crystals of the Al-10 Å phase than that in open system, indicating that H_2O plays a critical role in stabilizing the Al-10 Å phase. The lower amount of the Al-10 Å phase and lawsonite in the open system coincides with higher amounts of garnet and Na-clinopyroxene. The comparison of the experimental results at 3.5 and 4 GPa at the same temperature of 650 °C implies that the boundary between lawsonite blueschist and lawsonite eclogite is located at a pressure between 3.5 and 4 GPa. When the experimental temperature is increased to 750 °C at 4 GPa, all pre-existing hydrous minerals are decomposed within 120 h. The mineral assemblage mainly consists of garnet, Na-clinopyroxene, and coesite; only very little the Al-10 Å phase was observed in the central part of the sample near the platinum tube, where a local "closed" system persists in the open capsule. The Na-clinopyroxene from this run is almost homogeneous, in contrast to the heterogeneity at low temperature. Lawsonite disappeared completely. The experimental conditions approach the stability field of dry eclogite and the stability limit of the Al-10 Å phase should be close to 750 °C at 4 GPa.

At 5 GPa, we performed one experiment at 650 °C, which yielded the same mineral assemblage as the 4 GPa, 650 °C run—garnet, Na-clinopyroxene, the Al-10 Å phase, and minor lawsonite (5%). At a temperature of 650 °C, the amount of the Al-10 Å phase increased with pressure, from 5% at 4 GPa to 15% at 5 GPa.

At 5.5 GPa, we also carried out two experiments (BE-3-1 and BE-3-2) at 700 °C in different capsules (Fig. 3). The same mineral assemblage, consisting of garnet, heterogeneous Na-clinopyroxenes (Fig. 2c), the Al-10 Å phase, and minor lawsonite, were observed in both sealed and unsealed capsules. The experiment with sealed capsule produced more and bigger crystals of the Al-10 Å phase than with unsealed capsule (Fig. 3), similar to the observation of the experiments at 4 GPa and 650 °C. Higher water content in the system facilitated the formation of more and bigger the Al-10 Å phase. When the temperature increased to 800 °C, lawsonite and most of the Al-10 Å phase disappear with appearance of minor coesite, which is comparable to the result of the experiment at 4 GPa and 750 °C. At 900 °C, the Al-10 Å phase completely disappears and the amount of coesite increases to 10%. The observed mineral assemblage is consistent with dry eclogite, consisting of garnet, Na-clinopyroxene, and coesite.

At 7 GPa and 700 °C, the mineral assemblage consists predominantly of garnet and Na-clinopyroxene, with minor lawsonite and Al-10 Å phase (Fig. 2e). When the temperature increased to 750 °C, lawsonite and most of the Al-10 Å phase disappear with appearance of coesite. The Na-clinopyroxenes

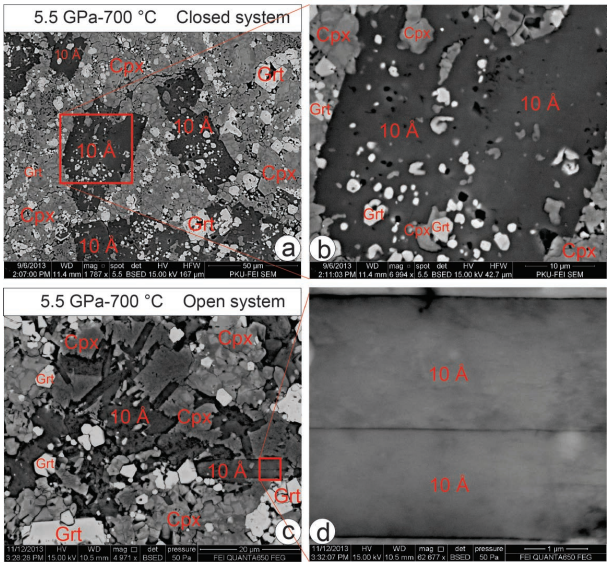

Figure 3. BSE images of run products at 5.5 GPa and 700 °C experiments in different capsules. (**a**) Run BE-3-2: Large Al-10 Å phase crystals with inclusions of garnet and omphacite also building up the matrix. (**b**) Al-10 Å phase with garnet and omphacite inclusions (enlarged view of **a**). (**c**) Run BE-3: Euhedral sheet-like Al-10 Å phase in a matrix of garnet and omphacite. (**d**) Sheet-like shaped Al-10 Å phase (enlarged view of **c**). (Color online.)

in the run product are homogeneous. The mineral assemblage at 8 GPa and 700 °C is the same as that at 7 GPa and 750 °C, indicating that dry eclogite is stable (Fig. 2f).

Mineral chemistry

The grain size of major minerals (garnet, Na-clinopyroxene, glaucophane, lawsonite, and the Al-10 Å phase) in the run products is above 10 μm, big enough to analyze their chemical composition with the electron microprobe. The mineral formulas were calculated from the microprobe data according to charge balance rules with the AX program (http://www.esc.cam.ac.uk/research/research-groups/holland/ax). A mica structure was chosen to calculate the mineral formula of the Al-10 Å phase given that the similar structure was refined by XRD data (see below).

Garnet. Garnet can be represented by four end-members: grossular (Grs), almandine (Alm), pyrope (Pyp), and spessartine (Sps). The garnets formed at low temperatures (≤800 °C) show weak compositional zoning (Supplemental[1] Table 3 and Fig. 2). Their cores have nearly the same compositions as the garnet in the starting material, which plot in the middle of the Grs-Sps-(Pyp+Alm) triangle diagram (Fig. 4a). In comparison to the rim, the cores are characterized by higher Mn content (Fig. 4a). The Ca content of garnet decreases with increasing pressure, while the sum of its Mg content increases with temperature (Fig. 4b). The charge-balance calculation showed garnets in the run products contains some Fe^{3+} contents, from 0 to 0.17 pfu; most of them containing 0.10 of Fe^{3+} pfu. The Fe^{3+} content of garnet may be a consequence of Fe alloyed with the Pt capsule causing oxidation of the sample (Merrill and Wyllie 1973; Johannes and Bode 1978).

Na-clinopyroxene. The experiments at low temperatures (≤700 °C) locally contains Na-clinopyroxenes with heterogeneous compositions (Supplemental[1] Table 4; Figs. 2b, 2c, 2e, and 4c). The compositional heterogeneity may be attributed to local disequilibrium at low temperature. The jadeite content of Na-clinopyroxene in this study is much higher than that in normal MORB composition at the same *P-T* condition because of higher Na_2O content in the starting material. The run products show considerable aegirine-augite (Fe^{3+}) content in Na-clinopyroxenes and andradite content in garnet, likely caused by alloyed Fe with Pt capsule. The experiments at high temperatures (≥800 °C) always show homogeneous Na-clinopyroxene (Fig. 2d).

Amphibole. Amphiboles only occur in the starting material and in the experiment at 3.5 GPa and 650 °C. All are Na-amphiboles (Fig. 4d). In the starting material, they show obvious compositional zoning, from glaucophane cores to crossite rims. The composition of Na-amphibole in the experimental run at 3.5 GPa and 650 °C is the same as the core composition of the starting material (Supplemental[1] Table 5; Fig. 4d). Compared with the compositionally zoned Na-amphibole in the starting

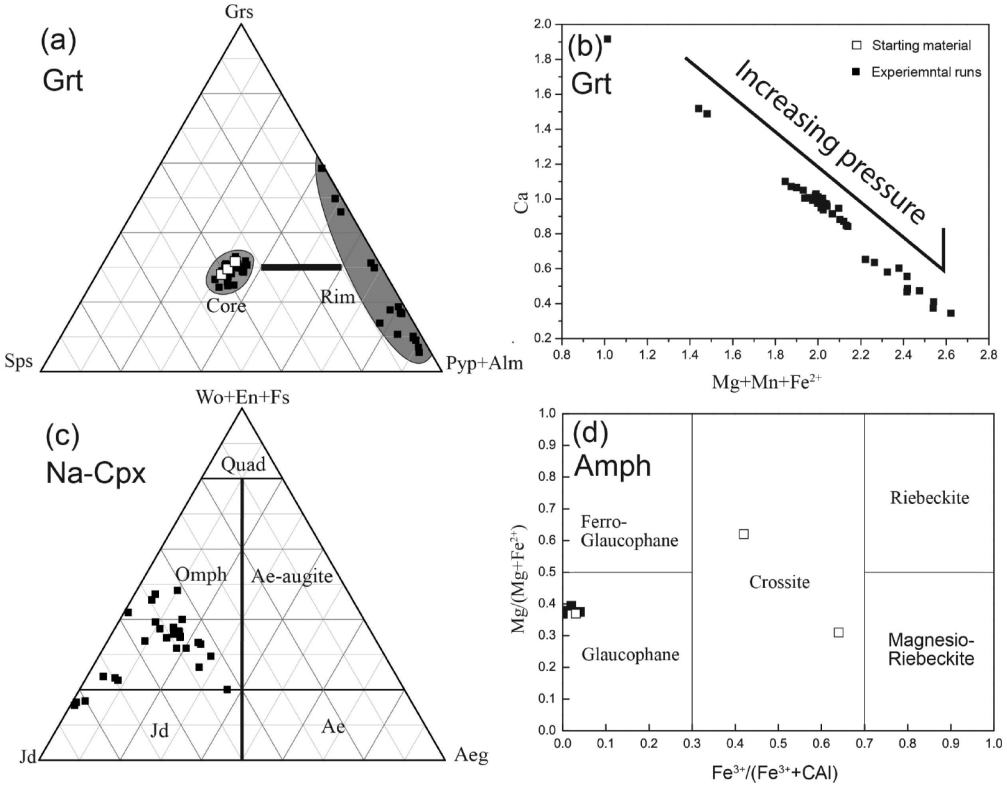

Figure 4. Compositional characteristics of garnet, Na-clinopyroxene, and amphibole in run products in comparison to that in the starting material. (**a**) Obvious compositional differences between garnet core and rim. (**b**) Substitution of Ca by (Mg+Fe+Mn) in garnet with increasing pressure. (**c**) Ternary jadeite (Jd); aegirine (Aeg); diopside (Wo+En+Fs); diagram after Morimoto et al. (1988) showing compositions of Na-clinopyroxene in the run products. (**d**) Classification of amphibole in run products and starting material in the $Mg/(Mg+Fe^{2+})$–$Fe^{3+}/(Fe^{3+}+CAl)$ diagram after Leake et al. (1997).

material, the Na-amphiboles in the experimental run are more homogenous and their compositions plot in the glaucophane region (Fig. 4d).

Lawsonite and epidote. Lawsonites in all experimental products are homogenous and the composition is close to the end-member mineral formula $[CaAl_2Si_2O_7(OH)_2 \cdot H_2O]$. Only minor Ca (<0.14 pfu) and Al (<0.11 pfu) are substituted by (Fe, Mg) and Si, respectively. A small amount of epidote formed in the experimental run at 3.5 GPa and 650 °C. In comparison to the end-member mineral formula of epidote $[Ca_2FeAl_2[SiO_4][Si_2O_7]O(OH)]$, the $Fe^{3+}/(Fe^{3+}+Al)$ ratio of epidote varies from 0.15 to 0.34. Some Ca in epidote is substituted by Fe^{2+}, similar to the substitution in lawsonite (Supplemental[1] Table 6).

The Al-10 Å phase

At pressures above 4 GPa, glaucophane completely disappeared and a new hydrous phase formed. The XRD data of the recovered sample from experiment (BE-3) at 5.5 GPa and 700 °C show a characteristic peak, which is similar to the phengite or the (Al-bearing) 10 Å phase (Fumagalli et al. 2001; Fumagalli and Poli 2005) (Supplemental[1] Fig. 2). The BSE images of this new phase also appear like a typical phyllosilicate (Fig. 3b), showing the layered structure of phengite or the 10 Å phase. However, the chemical composition of the new phase is different from neither those of phengite nor the 10 Å phase. The new phase has high-Al, -K, and -Si contents and low-Mg content, compared to the composition of the 10 Å phase (Supplemental[1] Table 7). The EMP analyses show low totals (81–94 wt%), likely reflecting variable H_2O contents (6–19 wt%). We used the phengite structure parameters (Smyth et al. 2000) to refine the lattice parameters of the new phase. The lattice parameters of the new phase (a = 5.1955 Å, b = 9.0705 Å, c = 20.1544 Å) were determined by Rietveld refinement of the XRD data of BE-3 (Fig. 5) using the GSAS software package (Larson and Von Dreele 2004). They are similar to the lattice parameters of hexagonal phengite (a = 5.32046 Å, b = 9.0368 Å, c = 19.8864 Å; Smyth et al. 2000). Compared with the structure parameters of the 10 Å phase (a = 5.3231 Å, b = 9.2031 Å, c = 10.2161 Å; Comodi et al. 2005), the c lattice parameter is almost doubled.

We calculated the mineral formulas of the new phase using the AX program assuming mica structure (Supplemental[1] Table 7). In comparison to phengite $[K(Mg,Fe)Al(Si_4O_{10})(OH)_2]$, the new phase has lower K contents (0.03–0.44 pfu) and contains more H_2O (6–19 wt%). The high-H_2O content would be more consistent with the (Al-bearing) 10 Å phase $[Mg_3(Si_4O_{10})(OH)_2 \cdot nH_2O]$ (Fumagalli et al. 2001; Fumagalli and Poli 2005). However, the $(Fe^{2+}+Mg)$ content of the new phase (<0.87 pfu) is much lower than those known for the 10 Å phase (= 3 pfu; Fumagalli et al. 2001), while its Al content is distinctly higher (= 1.32–2.02 pfu). Noticeably, the new phase always contains significant K, between 0.03 and 0.44 pfu. Given that the new phase has a similar structure to phengite (K-mica) and the 10 Å phase and that solid solution or mixed layering between phlogopite (K-mica) and the 10 Å phase is possible for low-K

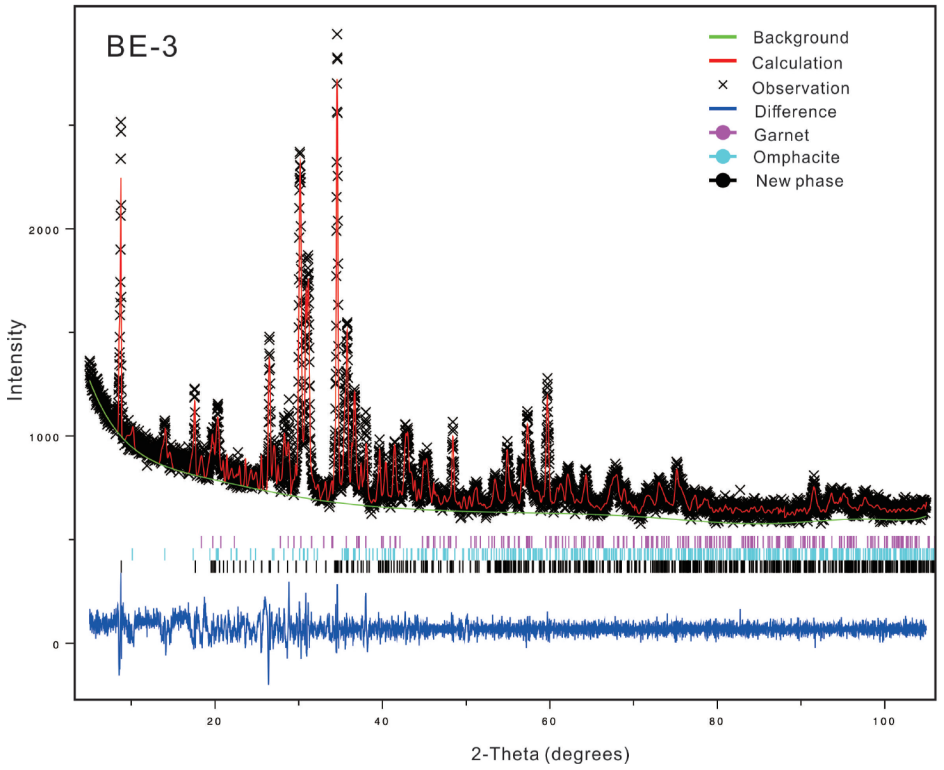

Figure 5. X-ray diffraction profile of run product (BE-3-1) at 5.5 GPa and 700 °C. The continuous red line is the calculated profile obtained by Rietveld refinement using the software package GSAS (Larson and Von Dreele 2004). Diffraction patterns of the phases present are: garnet; clinopyroxene, and new phase (Al-10 Å phase). (Color online.)

phlogopite (Fumagalli et al. 2009), we suggest the new phase, which is also a solid solutions or mixed layering between K-mica and the 10 Å phase. However, the new phase discovered here is not the conventional 10 Å phase, which is considered as the Mg-end-member of a solid solutions series. Here, we propose a substitution of 3(Mg+Fe^{2+}) by 2 Al on the octahedral site. Accordingly, the chemical composition of the new phase is closer to the composition of an Al-end-member (Supplemental[1] Table 7). We will therefore refer the new phase to "Al-10 Å phase" throughout the text and, for clear distinction, we will use "Mg-10 Å phase" for the conventional 10 Å phase hereafter. It is known that the Mg-10 Å phase can form in the talc, $Mg_3[Si_4O_{10}](OH)_2$, and H_2O system at 3–5 GPa through the reaction talc + H_2O = 10 Å phase (Pawley and Wood 1995; Chinnery et al. 1999). Accordingly, the Al-10 Å phase proposed in this study may be a high-pressure phase in the pyrophyllite, $Al_2[Si_4O_{10}](OH)_2$, and H_2O system. Further experiments are needed to verified this hypothesis.

Discussion

Formation and stability of the Al-10 Å phase in the MORB+H_2O system

All previous studies on the stability and the physical and chemical properties of the Mg-10 Å phase concerned the hydrated peridotite model system with emphasis on the MSH (MgO-SiO_2-H_2O) system. There is a limited understanding of the effect of CaO, Al_2O_3, FeO, Na_2O, and K_2O on the properties of the Mg-10 Å phase (Fumagalli et al. 2001; Comodi et al. 2005, 2006; Welch et al. 2006; Chollet et al. 2009; Pawley et al. 2010, 2011). So far, the Mg-10 Å phase has been thought to be present only in the hydrated ultramafic system at high pressure (Kawamoto 2006). In this study, we report a new (Al,K)-bearing 10 Å phase (Al-10 Å phase) formed in the hydrous mafic (MORB+H_2O) system. Given that the Mg-10 Å phase can be synthesized from talc in a water-saturated system at high pressure (Pawley and Wood 1995; Chinnery et al. 1999) and that talc is a common mineral in hydrous, low-temperature, and high-pressure metamorphic mafic rocks (especially of Mg-metagabbro) (Liou and Zhang 1995; Massonne 2004; Bucher and Grapes 2009; Wei and Clarke 2011), talc could transform into the Mg-10 Å phase in water-saturated metamafic rocks at higher pressure. The synthesis of the Al-10 Å phase in natural lawsonite blueschist in this study supports this hypothesis. The Al-10 Å phase synthesized in this study has distinctly high-Al_2O_3 content compared to the traditional Mg-10 Å phase. Fumagalli and Poli (2005) found notable Al_2O_3-content (about 10 wt%) in an Mg-10 Å phase in hydrous K-free peridotites (Na_2O-CaO-MgO-FeO-Al_2O_3-SiO_2 system); they suggested that complex interlayering between the Mg-10 Å phase and chlorite accounts for this peculiar mineral chemistry. The chemical composition of the starting material in this study has a much higher Al_2O_3 and lower (FeO+MgO) content (Supplemental[1] Table 1) than that of normal peridotite. The observed Al-10 Å phase is close to an Al-end-member. We expect a continuous solid solution on the octahedral site between the Mg-10 Å phase and the Al-10 Å phase. The Al_2O_3-bearing 10 Å phase reported in previous studies (Fumagalli and Poli 2005; Dvir et al. 2010) is likely an Al-bearing Mg-10 Å phase, while the Al-10 Å phase synthesized in this study is a Mg-bearing Al-10 Å phase.

To understand the formation of the Al-10 Å phase in the MORB+H_2O system, a ternary A[Al_2O_3]-C[CaO]-F[(Mg+FeO)] diagram (with SiO_2 and H_2O in excess) is utilized (Fig. 6). It illustrates typical protoliths of a wide range of metamorphic rocks (e.g., basaltic and ultrabasaltic rocks) and possible metamorphic minerals (e.g., lawsonite and 10 Å phase). Located on the side between the Al_2O_3 and (Mg+FeO) corners in the ACF diagram, the composition of the 10 Å phase varies from the Al-10 Å phase to the Mg-10 Å phase (Fig. 6). The chemical composition of the starting material of this study (lawsonite blueschist) plots in the ultrabasaltic rock field instead of the basaltic rock field, although its mineral assemblage and bulk composition were assigned to altered MORB. This is because starting material in this study contains much less CaO (4.2 wt%) and more Na_2O than normal altered basalts. In this study, the higher Na_2O content of the starting material can stabilize Na-amphibole to higher pressure (Pirard and Hermann 2015). The starting materials in this study are more consistent with ultrabasaltic than basaltic rocks if the effect of Na_2O on phase relations of Na_2O-free minerals in the experimental products can be ignored. Because the Mg-10 Å phase is common in hydrous Mg-rich ultrabasaltic rocks at high-pressure and low-temperature conditions, it is consequential that we synthesized the Al-10 Å phase in a hydrous, Al-rich but CaO-poor basaltic composition. Based on the experimental results in this study, Na_2O-rich amphibole (glaucophane) and lawsonite can be stable and are capable to carry K and H_2O to pressures up to 4 GPa. K and H_2O released by the decomposition of lawsonite and Na_2O-rich amphibole with increasing pressure was re-stored in the new K-bearing Al-10 Å phase. A possible reaction for the formation of the Al-10 Å phase can be simply determined by Schreinemakers rules in the ternary ACF diagram: lawsonite + $amphibole_{ss}$ = $pyroxene_{ss}$ + the 10 Å phase. The occurrence of this reaction is supported by local texture in our experimental runs showing the formation of the Al-10 Å phase around relic

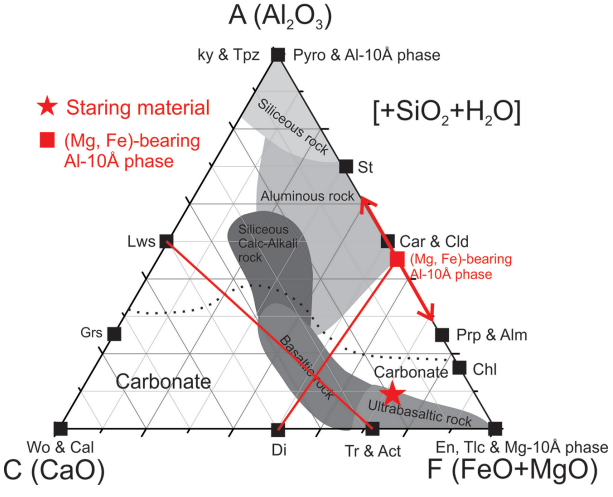

Figure 6. Ternary diagram in the system of A (Al_2O_3)–C(CaO)–F(FeO+MgO) with SiO_2 and H_2O in excess. Typical protoliths of metamorphic rocks and possible metamorphic minerals in this system (Bucher and Grapes 2011) are illustrated. The model chemical composition of starting material in this study (lawsonite blueschist) was plotted as red star in ultrabasaltic rock. (Color online.)

lawsonite (cf. Fig. 2c). The exact formation reaction of the Al-10 Å phase need further themodynamical calculation after we get enough data for the new phase.

The results of our high-pressure experiments defined the stability field of the Al-10 Å phase in the MORB+H_2O system (Fig. 7). The Al-10 Å phase appears in run products from 4 GPa, 650 °C via 5.5 GPa, 800 °C to 7 GPa, 750 °C (Supplemental[1] Table 2). The stability field of the Al-10 Å phase is distinctly broader than that of the Mg-10 Å phase in hydrated peridotite (Fumagalli and Poli 2005; Pawley et al. 2011) (Fig. 7). This work expands the stability region of the 10 Å phase from the ultramafic system to the mafic system, and highlights the significance of the 10 Å phase in deep H_2O- and K-cycles in subduction zones.

Possible solid solution/mixed layering between K-mica and the 10 Å phase on the interlayer site

Numerous studies have focused on the structure, stability, and dehydration of the Mg-10 Å phase (Fumagalli et al. 2001, 2005; Comodi et al. 2006; Welch et al. 2006; Fumagalli and Stixrude 2007; Chollet et al. 2009; Pawley et al. 2010, 2011). Both neutron powder diffraction on deuterated Mg-10 Å phase (Pawley et al. 2004) and X-ray powder diffraction (Fumagalli et al. 2001; Comodi et al. 2005) indicate that the Mg-10 Å phase has a phlogopite-type stacking structure. A possible mixed layering or solid solution between the Mg-10 Å phase and phlogopite has been used to explain the low-K content in phlogopite that was synthesized in a K-doped peridotite at low-temperature and high-pressure conditions (Fumagalli et al. 2009). We suggest that the Al-10 Å phase and phengite (K-mica) can also coalesce by continuous solid solution or mixed layering on the interlayer site.

To test the existence of solid solution or mixed layering between mica and the 10 Å phase at the 12-fold-coordinated site, we plotted previously reported compositions of natural and synthetic micas and (Al-bearing) 10 Å phases in a (Ca+Na)-K-H_2O triangular diagram (Fig. 8). The triangular diagram shows continuous composition between the 10 Å phase and K-mica, but a distinct gap between Na-mica and K-mica, consistent with the previously reported coexistence of paragonite and phengite in blueschist and eclogite (Ahn et al. 1985). The limited data available do not permit conclusions on the compositional variation between Na-mica and the 10 Å phase. Previous studies also have paid some attentions on non-stoichiometric K on the 12-fold-coordinated site of micas (as low as 0.7 pfu), especially for those formed at low temperatures and high pressures (Wang and Banno 1987; Torre et al. 1996; Lü et al. 2008). The illite/talc substitution [$K^{XII} + Al^{IV} = \square^{XII} + Si^{IV}$] has been proposed to explain non-stoichiometric K on the 12-fold-coordinated site of micas, based on study of the miscellaneous isomorphous substitution in K white micas (Wang and Banno 1987; Guidotti and Sassi 1998, 2002; Fumagalli et al. 2009). However, the model of vacancies on the 12-fold-coordinated site cannot explain "excess" water and low-K content in some K-micas from typical metamorphic rocks (Hervig and Peacock 1989) and in the Al-10 Å phase in this study. Fumagalli et al. (2009) suggested a possible 10 Å phase substitution ($K^{XII} + Al^{IV} = H_2O^{XII} + Si^{IV}$) to explain the high water and low (K+Na) content in phlogopite from metasomatized peridotites. We plotted previously reported composition of synthetic or natural micas and 10 Å phases in a (Na+K)/(Na+K+H_2O)-Si diagram (Fig. 9). The three end-members (red filled circles) of this diagram are mica, phengite, and 10 Å phase. There are two evolutional trends during increasing pressure, the substitution $Al^{VI} + Al^{IV} = Mg^{VI} + Si^{IV}$ at relatively high temperature, and the substitution $K^{XII} + Al^{IV} = H_2O^{XII} + Si^{IV}$ at relatively low temperature. Both can cause the increase of the Si content in mica with pressure. However, molecular H_2O can be brought into the mica structure only at relatively low temperatures and high pressures (Fig. 9). The substitution $K^{XII} + Al^{IV} = H_2O^{XII} + Si^{IV}$ can also explain why the K_2O content in phengite decreases with increasing bulk H_2O content at subsolidus conditions (Rosenthal and Frost 2014). The observation supports that the mica-10 Å phase solid solution or mixed layering at the 12-fold-coordinated site forms a continuous series and its composition shifts to the 10 Å phase end-member at high pressures, especially at low temperatures. Further detailed structure studies (XRD and TEM) are needed to better understand the structure evolution between K-mica and the 10 Å phase.

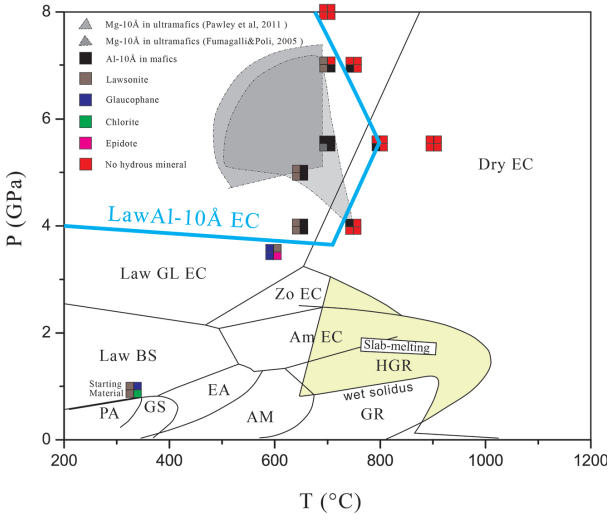

FIGURE 7. Experimentally constrained stability region of the Al-10 Å phase in this study in comparison to stability regions of the Mg-10 Å phase in the hydrated peridotite system in previous studies. Metamorphic facies boundaries experimentally derived for the MORB+H_2O system are taken from Okamoto and Maruyama (1999). Hydrous phases in the starting material and run products are marked with different colors. (Color online.)

The effect of f_{H_2O} on the Al-10 Å phase

We conducted experiments with sealed and unsealed capsules to understand the effect of the water fugacity (f_{H_2O}) on the formation and composition of the Al-10 Å phase. The sealed platinum capsule represents a relatively closed system, while the unsealed platinum tube with diamond powder represents a relatively open system. From 4 to 5.5 GPa, the amount of lawsonite decreased, while the amount of the Al-10 Å phase increased. At 4 GPa and 650 °C, the Al-10 Å phase forms relatively small grains (less than 10 μm) in the run products of both open and closed systems. However, the amount of the Al-10 Å phase formed in the open system is about 5%, much lower than that in the in closed system (15%). At 5.5 GPa and

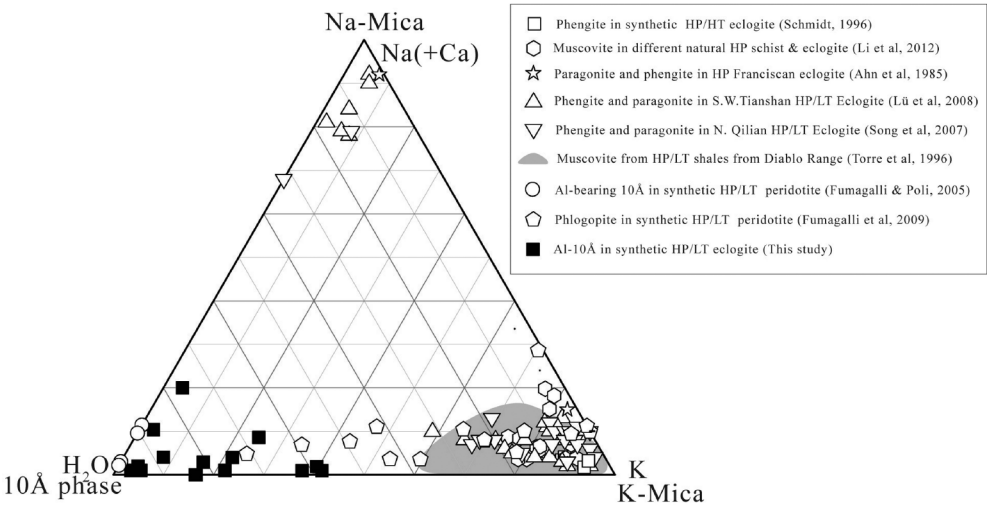

FIGURE 8. Triangular (Ca+Na)–K–H_2O diagram for the 12-fold-coordinated site of reported natural or synthetic mica and 10 Å phase. The H_2O content on the 12-fold-coordinated site is calculated assuming (Ca+Na)+K+H_2O = 1. Natural mica from HP/LT metamorphic rocks has higher H_2O content on the 12-fold-coordinated site than that from LP/HT ones.

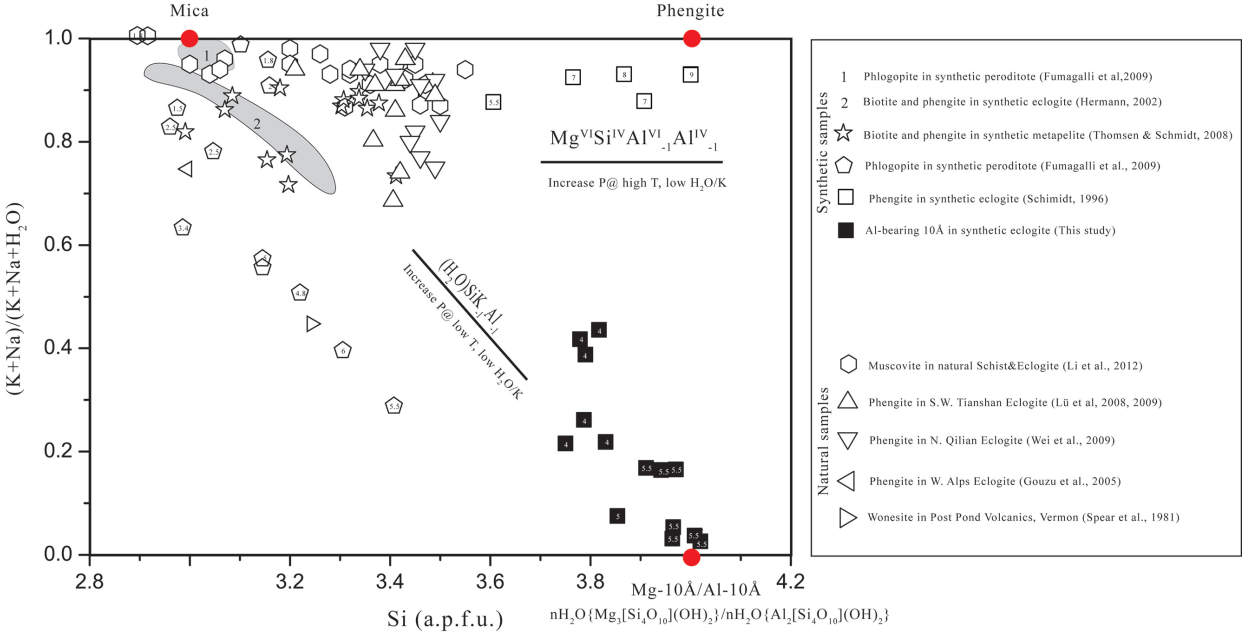

FIGURE 9. (K+Na)/(K+Na+H_2O) on the 12-fold-coordinated site vs. Si of previously reported natural or synthetic mica and 10 Å phase. There are two compositional evolution trends for mica (phlogopite and biotite) at low pressure: Substitution ($Al^{VI}+Al^{IV} = Mg^{VI}+Si^{IV}$). (2) Substitution ($K^{XII}+Al^{IV} = H_2O^{XII}+Si^{IV}$). For synthetic micas, the experimental pressures are marked in the icon. (Color online.)

700 °C, the amount of the Al-10 Å phase increases to 15% in the open system and to 25% in the closed system.

At 5.5 GPa and 700 °C, the grain sizes of the Al-10 Å phase are larger in the closed than in the open system. For example, grains of the Al-10 Å phase in the closed system grow to 50 μm across. The large Al-10 Å phase crystals always contain small Na-clinopyroxene and garnet inclusions (Figs. 3a and 3b). However, in the open system, the Al-10 Å phase is characterized by euhedral sheets of about 15 μm length and about 5 μm width (Figs. 3c and 3d). The composition of the Al-10 Å phase also differs between the open and closed systems, with a higher K but lower H_2O content in the open system (Supplemental[1] Table 7). It is expected that the f_{H_2O} is higher in the closed system than in the open system. High f_{H_2O} enhances the formation of the Al-10 Å phase and crystal growth. It also leads to high-H_2O/K ratio on the 12-fold-coordinated site.

IMPLICATIONS

K-micas (muscovite and phlogopite) are the principal H_2O and K hosts in the crust. They play a key role in deep H_2O and K cycles in subduction zones and Earth's upper mantle. As discussed, it is evident that the properties of the solid solution/mixed layering between K-mica and the 10 Å phase are controlled by the H_2O/K ratio, pressure and temperature conditions. From the subduction zone perspective, the K cycle in the subduction zone should be coupled with the H_2O cycle, especially in cold subduction zones. The starting material in this study contains 0.16 wt% K_2O, representing the normal oceanic crust composition. All K_2O is hosted by glaucophane in the starting material. Along cold subduction path, glaucophane will disintegrate completely and liberate the bulk K_2O and significant H_2O. Meanwhile, the subducted basaltic rock will transform into lawsonite and/or Al-10 Å phase eclogite, and most K and H_2O released by glaucophane decomposition will be re-stored in the solid solution/mixed layering of K-mica and 10 Å phase. This differs from the previous conclusion that descending oceanic crust releases all its K when amphibole breaks down during relatively hot subduction (Tatsumi 1989; Tatsumi and Eggins 1995).

We plotted typical *P-T* paths of cold, warm, and hot subduction on a phase diagram for the MORB+H_2O system (Okamoto and Maruyama 1999) together with the stability regions of phengite (Schmidt 1996) and the Al-10 Å phase (this study) to discuss the coupled K and H_2O cycles in different subduction scenarios (Fig. 10). Before the onset of subduction, the bulk K in an altered MORB is stored in amphibole or mica. Along the hot subduction path, all K will be released from the down-going slab due to dehydration melting of amphibole or mica at depths less than 50 km. In this scenario, K cannot be transported into Earth's mantle beyond 50 km. On the other hand, in a cold subduction zone, K in micas will remain in phengite, while K in amphibole will be released by amphibole decomposition at depths of 80–100 km and be restored in the solid solution/mixed layering of phengite and the 10 Å phase. The solid solution/mixed layering of phengite and the Al-10 Å phase will be stable up to 8 GPa and then decompose into K-hollandite and a K-rich fluid. Some K will be released from the subducted crust dissolved in fluid, while other K will be incorporated into K-bearing omphacite through the reaction phengite = $KAlSi_2O_6$ – clinopyroxene + enstatite + coesite + K-rich fluid and transported into deeper mantle (Schmidt 1996). The K- and H_2O-cycles in subduction regimes along hot or cold path should be between both scenarios. For the example of a warm slab (Fig. 10), most of the K in amphibole will be released into the fluid with amphibole decomposition at a depth of about 100 km, while the release of the K in phengite always depends on the intersection of the subduction path and the K-bearing MORB solidus. Of course, K can partly be restored into K-omphacite and transported into Earth's deeper mantle. The amount of K stored in K-omphacite is controlled by the pressure and the amount of omphacite in the subduction zone (Schmidt 1996; Han et al. 2015).

According to the discussion on the effect of f_{H_2O} on the Al-10 Å phase, the H_2O/K ratio can also play a significant role in the coupled H_2O- and K-cycle in the subduction zone. The higher the H_2O content in the system, the more Al-10 Å phase will be produced, leading to more bulk K and H_2O into deeper mantle by

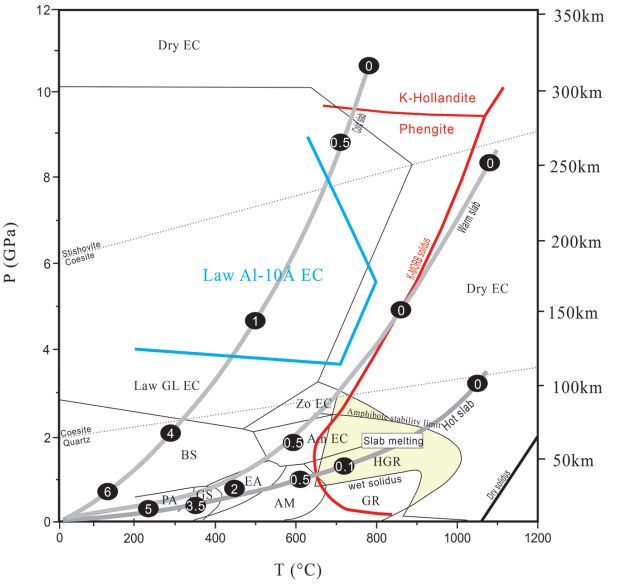

FIGURE 10. Comparison of the stability regions of the Al-10 Å phase (this study) and phengite (Schmidt 1996) in the MORB+H_2O system. Metamorphic facies boundaries experimentally derived for the MORB+H_2O system are taken from Okamoto and Maruyama (1999). The blue line shows the stability region of the Al-10 Å phase obtained in this study; the red line shows the stability region of phengite. Typical hot, warm, and cold subduction paths (light gray arrows) are taken from Okamoto and Maruyama (1999) and Schmidt (1996). The water contents along different subduction paths are marked in the black solid circle (Okamoto and Maruyama 1999). (Color online.)

the K-bearing Al-10 Å phase. If the H_2O content of the system is low, all of its bulk K could be stored in phengite and released by decomposition or melting of phengite with increasing pressure and temperature. According to previous thermodynamic calculations and high-pressure experimental constraints of phase relations (Maruyama and Okamoto 2007; Wei and Clarke 2011), the subducted basaltic rocks can host and bring much more H_2O into Earth's mantle in cold subduction zones than in hot ones. The high f_{H_2O} in a cold subduction zone will generally enhance the bulk K transportation to deep mantle through the Al-10 Å phase.

ACKNOWLEDGMENTS

This work was supported by the National Natural Science Foundation of China (41330210; 41520104004; 41502038; 41272069; 41350110224) and the China Postdoctoral Science Fundation (2015M570009). We thank Xiang Wu, Chunjing Wei, reviewers (Alison Pawley and an anonymous reviewer) and editor (Oliver Tschauner) for their constructive suggestions, and Ye Wu, Qiang He, Fei Wang, Hejing Wang and Xiaoli Li for their assistance with instruments used in this study.

REFERENCES CITED

Ahn, J.H., Peacor, D.R., and Essene, E.J. (1985) Coexisting paragonite-phengite in blueschist eclogite: A TEM study. American Mineralogist, 70, 1193–1204.

Alt, J.C. (1995) Subseafloor processes in mid-ocean ridge hydrothermal systems. Seafloor hydrothermal systems. In S.E. Humphris, R. Zierenberg, L. Mullineaux, and R. Thomson, Eds., Physical, Chemical, Biological and Geological Interactions within Hydrothermal Systems, 91, 85–114. American Geophysical Union, Washington, D.C.

Bauer, J.F., and Sclcar, C.B. (1981) The "10 Å phase" in the system MgO-SiO_2-H_2O. American Mineralogist, 66, 576–585.

Brown, M. (2006) Duality of thermal regimes is the distinctive characteristic of plate tectonics since the Neoarchean. Geology, 34, 961–964.

Bucher, K., and Grapes, R. (2009) The eclogite-facies Allalin gabbro of the Zermatt-

Saas ophiolite, western Alps: A record of subduction zone hydration. Jounal of Petrology, 50, 1405–1442.
——— (2011) Petrogenesis of Metamorphic Rocks, 345p. Springer, New York.
Chinnery, N.J., Pawley, A.R., and Clark, S.M. (1999) In situ observation of the formation of 10 Å phase from talc + H_2O at mantle pressures and temperatures. Science, 286, 940–942.
Chollet, M., Daniel, I., Koga, K.T., Petitgirard, S., and Morard, G. (2009) Dehydration kinetics of talc and 10 Å phase: Consequences for subduction zone seismicity. Earth and Planetary Science Letters, 284, 57–64.
Clarke, G.L., Powell, R., and Fitzherbert, J.A. (2006) The lawsonite paradox: A comparison of field evidence and mineral equilibria modelling. Journal of Metamorphic Geology, 24, 715–725.
Comodi, P., Fumagalli, P., Nazzareni, S., and Zanazzi, P.F. (2005) The 10 Å phase: Crystal structure from single-crystal X-ray data. American Mineralogist, 90, 1012–1016.
Comodi, P., Cera, F., Dubrovinsky, L., and Nazzareni, S. (2006) The high-pressure behaviour of the 10 Å phase: A spectroscopic and diffractometric study up to 42 GPa. Earth and Planetary Science Letters, 246, 444–457.
Dickinson, W.R., and Hatherton, T. (1967) Andesitic volcanism and seismicity around the Pacific. Science, 157, 801–803.
Domanik, K.J., and Holloway, J.R. (1996) The stability and composition of phengitic muscovite and associated phases from 5.5 to 11 GPa: Implications for deeply subducted sediments. Geochimica et Cosmochimica Acta, 60, 4133–4150.
Dvir, O., Pettke, T., Fumagalli, P., and Kessel, R. (2010) Fluids in the peridotite-water system up to 6 GPa and 800 °C: New experimental constrains on dehydration reactions. Contributions to Mineralogy and Petrology, 161, 829–844.
Fumagalli, P., and Poli, S. (2005) Experimentally determined phase relations in hydrous peridotites to 6.5 GPa and their consequences on the dynamics of subduction zones. Journal of Petrology, 46, 555–578.
Fumagalli, P., and Stixrude, L. (2007) The 10 Å phase at high pressure by first principles calculations and implications for the petrology of subduction zones. Earth and Planetary Science Letters, 260, 212–226.
Fumagalli, P., Stixrude, L., Poli, S., and Snyder, D. (2001) The 10 Å phase: A high-pressure expandable sheet silicate stable during subduction of hydrated lithosphere. Earth and Planetary Science Letters, 186, 125–141.
Fumagalli, P., Zanchetta, S., and Poli, S. (2009) Alkali in phlogopite and amphibole and their effects on phase relations in metasomatized peridotites: A high-pressure study. Contributions to Mineralogy and Petrology, 158, 723–737.
Gouzu, C., Itaya, T., and Takeshita, H. (2005) Interlayer cation vacancies of phengites in calcschists from the Piemonte zone, western Alps, Italy. Journal of Mineralogical and Petrological Sciences, 100, 143–149.
Guidotti, C.V., and Sassi, F.P. (1998) Miscellaneous isomorphous substitutions in Na-K white micas: a review, with special emphasis to metamorphic micas. Rendiconti Lincei Scienze Fisiche e Naturali, 9, 57–78.
——— (2002) Constraints on studies of metamorphic K-Na white micas. Reviews in Mineralogy and Geochemistry, 46, 413–448.
Hacker, B.R. (2008) H_2O subduction beyond arcs. Geochemistry, Geophysics, Geosystems, 9, Q03001.
Han, L., Zhang, L., and Zhang, G. (2015) Ultra-deep subduction of Yematan eclogite in the North Qaidam UHP belt, NW China: Evidence from phengite exsolution in omphacite. American Mineralogist, 100, 1848–1855.
Hermann, J. (2002) Experimental constraints on phase relations in subducted continental crust. Contributions to Mineralogy and Petrology, 143, 219–235.
Hervig, R.L., and Peacock, S.M. (1989) Water and trace elements in coexisting muscovite and biotite from metamorphic rocks. EOS, Transactions, American Geophysical Union, 70, 490.
Johannes, W., and Bode, B. (1978) Loss of iron to the Pt-container in melting experiments with basalts and a method to reduce it. Contributions to Mineralogy and Petrology, 67, 221–225.
Kawamoto, T. (2006) Hydrous phases and water transport in the subducting slab. Reviews in Mineralogy and Geochemistry, 62, 273–289.
Kogiso, T., Tatsumi, Y., and Nakano, S. (1997) Trace element transport during dehydration processes in the subducted oceanic crust 1. Experiments and implications for the origin of ocean island basalts. Earth and Planetary Science Letters, 148, 193–205.
Konzett, J., and Fei, Y. (2000) Transport and storage of potassium in the Earth's upper mantle and transition zone: an experimental study to 23 GPa in simplified and natural bulk compositions. Journal of Petrology, 41, 583–603.
Konzett, J., and Ulmer, P. (1999) The stability of hydrous potassic phases in lherzolitic mantle-an experimental study to 9.5 GPa in simplified and natural bulk compositions. Journal of Petrology, 40, 629–652.
Larson, A.C., and Von Dreele, R.B.V. (2004) General Structure Analysis System (GSAS). Los Alamos National Laboratory Report, LAUR 86-748.
Leake, B.E., Woolley, A.R., Arps, C.E.S., Birch, W.D., Gilbert, M.C., Grice, J.D., Hawthorne, F.C., Kato, A., Kisch, H.J., Krivovichev, V.G., Linthout, K., Laird, J., Mandarino, J.A., Maresch, W.V., Nickel, E.H., Rock, N.M.S., Schumacher, J.C., Smith, D.C., Stephenson, N.C.N., Ungaretti, L., Whittaker, E.J.W., and Guo, Y.Z. (1997) Nomenclature of amphiboles: Report of the subcommittee on amphiboles of the International Mineralogical Association, commission on new minerals and mineral names. American Mineralogist, 82, 1019–1037.
Li, H., Zhang, L., and Christy, A.G. (2011) The correlation between Raman spectra and the mineral composition of muscovite and phengite. In L. Dobrzhinetskaya, S. Wali, S. Faryad, S. Wallis, and S. Cuthbert, Eds., 25 years after first discovery of coesite and diamond, 7, 187–212. Elsevier, London.
Liou, J.G., and Zhang, R.Y. (1995) Significance of ultrahigh-P talc-bearing eclogitic assemblages. Mineralogical Magazine, 59, 93–102.
Liu, X., Chen, J., Tang, J., He, Q., Li, S., Peng, F., He, D., Zhang, L., and Fei, Y. (2012a) A large volume cubic press with a pressure-generating capability up to about 10 GPa. High Pressure Research: An International Journal, 32, 239–254.
Liu, X., Wang, S., He, Q., Chen, J., Wang, H., Li, S., Peng, F., Zhang, L., and Fei, Y. (2012b) Thermal elastic behavior of $CaSiO_3$-walstromite: A powder X-ray diffraction study up to 900 °C. American Mineralogist, 97, 262–267.
Lü, Z., Zhang, L., Du, J., and Bucher, K. (2008) Coesite inclusions in garnet from eclogitic rocks in western Tianshan, northwest China: Convincing proof of UHP metamorphism. American Mineralogist, 93, 1845–1850.
Mallik, A., Nelson, J., and Dasgupta, R. (2015) Partial melting of fertile peridotite fluxed by hydrous rhyolitic melt at 2–3 GPa: Implications for mantle wedge hybridization by sediment melt and generation of ultrapotassic magmas in convergent margins. Contributions to Mineralogy and Petrology, 169, 48.
Maruyama, S., and Okamoto, K. (2007) Water transportation from the subducting slab into the mantle transition zone. Gondwana Research, 11, 148–165.
Maruyama, S., Liou, J.G., and Terabayashi, M. (1996) Blueschists and eclogites of the world and their exhumation. International Geology Review, 38, 485–594.
Massonne, H.J. (2004) A low-variance mineral assemblage with talc and phengite in an eclogite from the Saxonian Erzgebirge, Central Europe, and its *P-T* evolution. Journal of Petrology, 46, 355–375.
McDonough, W.F. (2014) Compositional model for the Earth's core. In H.D. Holland and K.K. Turekian, Eds., Treatise on Geochemistry, 2nd ed., 2, 559–577.
Merrill, R.B., and Wyllie, P.J. (1973) Absorption of iron by platinum capsules in high pressure rock melting experiments. American Mineralogist, 58, 16–20.
Miyashiro, A. (1973) Metamorphism and Metamorphic Belts, 492 p. Allen and Unwin, London.
Morimoto, N., Fabries, J., Ferguson, A.K., Ginzburg, I.V., Ross, M., Seifert, F.A., Zussman, J., Aoki, K., and Gottardi, G. (1988) Nomenclature of pyroxenes. American Mineralogist, 73, 1123–1133.
Okamoto, K., and Maruyama, S. (1999) The high-pressure synthesis of lawsonite in the MORB+H_2O system. American Mineralogist, 84, 362–373.
Padrón-Navarta, J.A., Tommasi, A., Garrido, C.J., Sánchez-Vizcaíno, V.L., Gómez-Pugnaire, M.T., Jabaloy, A., and Vauchez, A. (2010) Fluid transfer into the wedge controlled by high-pressure hydrofracturing in the cold top-slab mantle. Earth and Planetary Science Letters, 297, 271–286.
Pawley, A.R., and Wood, B.J. (1995) The high-pressure stability of talc and 10 Å phase: Potential storage sites for H_2O in subduction zones. American Mineralogist, 80, 998–1003.
Pawley, A.R., Welch, M.D., and Smith, R.I. (2004) The 10-Å phase: Structural constrains from neutron powder diffraction. Lithos, 73, S86.
Pawley, A.R., Welch, M.D., Lennie, A.R., and Jones, R.L. (2010) Volume behavior of the 10 Å phase at high pressures and temperatures, with implications for H_2O content. American Mineralogist, 95, 1671–1678.
Pawley, A.R., Chinnery, N.J., Clark, S.M., and Walter, M.J. (2011) Experimental study of the dehydration of 10-Å phase, with implications for its H_2O content and stability in subducted lithosphere. Contributions to Mineralogy and Petrology, 162, 1279–1289.
Peacock, S.M., and Wang, K. (1999) Seismic consequences of warm versus cool subduction metamorphism: examples from Southwest and Northeast Japan. Science, 286, 937–939.
Pirard, C., and Hermann, J. (2015) Experimentally determined stability of alkali amphibole in metasomatised dunite at sub-arc pressures. Contributions to Mineralogy and Petrology, 169, 1–26.
Poli, S., and Schmidt, M.W. (2002) Petrology of subducted slabs. Annual Review of Earth and Planetary Sciences, 30, 207–235.
Rampone, E., and Morten, L. (2001) Records of crustal metasomatism in the garnet peridotites of the Ulten Zone (Upper Austroalpine, Eastern Alps). Journal of Petrology, 42, 207–219.
Ringwood, A.E. (1974) The petrological evolution of island arc systems: Twenty-seventh William Smith Lecture. Journal of the Geological Society, 130, 183–204.
Rosenthal, A., and Frost, D.J. (2014) High pressure experimental constraints on the fate of water during subduciton of oceanic crustal material into deep mantle. Geophysical Research Abstracts, 16, 16070.
Schmidt, M.W. (1995) Lawsonite: Upper pressure stability and formation of higher density hydrous phases. American Mineralogist, 80, 1286–1292.
——— (1996) Experimental constraints on recycling of potassium from subducted oceanic crust. Science, 272, 1927–1929.
Schmidt, M.W., and Poli, S. (1998) Experimentally based water budgets for dehydrating slabs and consequences for arc magma generation. Earth and Planetary Science Letters, 163, 361–379.
——— (2014) Devolatilization during subduction. In H.D. Holland and K.K.

Turekian, Eds., Treatise on Geochemistry 2nd ed., 4, 669–701. Elsevier.
Smyth, J.R., Jacobsen, S.D., Swope, R.J., Angel, R.J., Alt, T., Domanik, K., and Holloway, J.R. (2000) Crystal structures and compressibilities of synthetic $2M_1$ and $3T$ phengite micas. European Journal of Mineralogy, 12, 955–963.
Song, S., Zhang, L., Niu, Y., Su, L., Song, B., and Liu, D. (2005) Evolution from oceanic subduction to continental collision: a case study from the northern Tibetan plateau based on geochemical and geochronological data. Journal of Petrology, 47, 435–455.
Song, S.G., Zhang, L.F., Niu, Y., Wei, C.J., Liou, J.G., and Shu, G.M. (2007) Eclogite and carpholite-bearing metasedimentary rocks in the North Qilian suture zone, NW China: Implications for Early Palaeozoic cold oceanic subduction and water transport into mantle. Journal of Metamorphic Geology, 25, 547–563.
Spear, F.S., Hazen, R.M., and Rumble, D.R. III (1981) Wonesite: a new rock-forming silicate from the Post Pond Volcanics, Vermont. American Mineralogist, 66, 100–105.
Staudigel, H. (2014) Chemical fluxes from hydrothermal alteration of the oceanic crust. In H.D. Holland and K.K. Turekian, Eds., Treatise on Geochemistry 2nd ed., 4, 583–606.
Syracuse, E.M., van Keken, P.E., and Abers, G.A. (2010) The global range of subduction zone thermal models. Physics of the Earth and Planetary Interiors, 183, 73–90.
Tamura, Y., Tani, K., Chang, Q., Shukuno, H., Kawabata, H., Ishizuka, O., and Fiske, R.S. (2007) Wet and dry basalt magma evolution at Torishima volcano, Izu Bonin Arc, Japan: The possible role of phengite in the down going slab. Journal of Petrology, 48, 1999–2031.
Tatsumi, Y. (1989) Migration of fluid phases and genesis of basalt magmas in subduction zones. Journal of Geophysical Research, 94, 4697.
Tatsumi, Y., and Eggins, S.M. (1995) Subduction zone magmatism. Surveys in Geophysics, 5, 535–536.
Torre, M.D., Livi, K.J.T., Veblen, D.R., and Frey, M. (1996) White K-mica evolution from phengite to muscovite in shales and shale matrix melange, Diablo Range, California. Contributions to Mineralogy and Petrology, 123, 390–405.
Tsujimori, T., and Ernst, W.G. (2014) Lawsonite blueschists and lawsonite eclogites as proxies for paleo-subduction zone processes: A review. Journal of Metamorphic Geology, 32, 437–454.
Tsujimori, T., Sisson, V., Liou, J., Harlow, G., and Sorensen, S. (2006) Very-low-temperature record of the subduction process: A review of worldwide lawsonite eclogites. Lithos, 92, 609–624.
Van Keken, P.E., Hacker, B.R., Syracuse, E.M., and Abers, G.A. (2011) Subduction factory: 4. Depth-dependent flux of H_2O from subducting slabs worldwide. Journal of Geophysical Research, 116, B1.
van Roermund, H.L.M., Carlswell, D.A., Drury, M.R., and Heijboer, T.C. (2002) Microdiamonds in a megacrysts garnet websterite pod from Bardane on the island of Fjørtoft, wesytren Norway: Evidence for diamond formation in mantle rocks during deep continental subduction. Geology, 30, 959–962.
Wang, G-.F., and Banno, S. (1987) Non-stoichiometry of interlayer cations in micas from low- to middle-grade metamorphic rocks in the Ryoke and the Sanbagawa belts, Japan. Contributions to Mineralogy and Petrology, 97, 313–319.
Wang, J., Kalinichev, A.G., and Kirkpatrick, R.J. (2004) Molecular modeling of the 10-Å phase at subduction zone conditions. Earth and Planetary Science Letters, 222, 517–527.
Wei, C.J., and Clarke, G.L. (2011) Calculated phase equilibria for MORB compositions: a reappraisal of the metamorphic evolution of lawsonite eclogite. Journal of Metamorphic Geology, 29, 939–952.
Wei, C.J., Yang, Y., Su, X.L., Song, S.G., and Zhang, L.F. (2009) Metamorphic evolution of low-Teclogite from the North Qilian orogen, NW China: evidence from petrology and calculated phase equilibria in the system NCKFMASHO. Journal of Metamorphic Geology, 27, 55–70.
Welch, M.D., Pawley, A.R., Ashbrook, S.E., Mason, H.E., and Phillips, B.L. (2006) Si vacancies in the 10 Å phase. American Mineralogist, 91, 1707–1710.
Whitney, D.L., and Davis, P.B. (2006) Why is lawsonite eclogite so rare? Metamorphism and preservation of lawsonite eclogite, Sivrihisar, Turkey. Geology, 34, 473–476.
Whitney, D.L., and Evans, B.W. (2009) Abbreviations for names of rock-forming minerals. American Mineralogist, 95, 185–187.
Wunder, B., and Melzer, S. (2003) Experimental evidence on phlogopitic mantle metasomatism induced by phengite dehydration. European Journal of Mineralogy, 15, 641–647.
Wyllie, P.J. (1988) Magma genesis, plate tectonics, and chemical differentiation of the Earth. Reviews of Geophysicas, 26, 370–404.
Zhang, R.Y., Li, T., Rumble, D., Yui, T.F., Li, L., Yang, J.S., Pan, Y., and Liou, J.G. (2007) Multiple metasomatism in Sulu ultrahigh-P garnet peridotite constrained by petrological and geochemical investigations. Journal of Metamorphic Geology, 25, 149–164.
Zhang, L., Wang, Q., and Song, S. (2009) Lawsonite blueschist in Northern Qilian, NW China: P–T pseudosections and petrologic implications. Journal of Asian Earth Sciences, 35, 354–366.

Manuscript received November 19, 2016
Manuscript accepted May 4, 2017
Manuscript handled by Oliver Tschauner